

# Zero-Copy Semantic Contagion: An In-Memory Streaming Architecture for Evolving Attention Graphs \*

Kabir Murjani

Department of Electrical Engineering  
Nirma University  
Ahmedabad, India  
23bee064@nirmauni.ac.in

## Abstract

Per-ticker forecasting models dominate financial time-series work yet remain blind to cross-company propagation: a foundry disruption in Taiwan does not register in a single-asset model until Apple’s own price has already moved. To address this limitation, we introduce a heterogeneous Rust-Python streaming architecture that maps cross-company attention as a continuous-time graph driven directly from text. We show that on the ingestion side, a zero-copy Rust edge parses news records in  $\sim 100$  ns and scans the target equity universe in  $\sim 1.2 \mu$ s. On the inference end, a multivariate Neural Hawkes Process featuring per-node continuous-time LSTM states and a bilinear latent projection propagates directed excitation, while an adaptive pruning rule bounds the computational cost of dynamic neighborhood updates. Combining these stages, we demonstrate an end-to-end processing latency of  $\sim 13$  ms per incoming news record on a single commodity CPU. Evaluated on a one-month temporal holdout of the FNSPID corpus (638 articles across 47 tickers), the system delivers a  $1.70\times$  precision lift over random at the 90th-percentile next-day return threshold, and  $3.36\times$  over a same-sector baseline. Crucially, removing the graph topology collapses precision to zero, confirming that the dynamic attention network is the sole driver of cross-company signal in this architecture.

## CCS Concepts

- **Information systems**  $\rightarrow$  **Data streaming**; *Data stream mining*;
- **Computing methodologies**  $\rightarrow$  **Neural networks**.

## Keywords

Hawkes processes, semantic contagion, zero-copy parsing, continuous-time graphs, market microstructure

## 1 Introduction

The efficient-market hypothesis [1] predicts that prices absorb new information without delay, but the empirical microstructure tells a more nuanced story [2]. Numerical signals—price ticks, volume jumps, order-book imbalances that are arbitrated in microseconds by automated systems [3]. Qualitative information, on the contrary, must first be parsed into semantic content before it can move prices, and the resulting impact unfolds over a 20–60 minute horizon [4, 5].

What this asymmetry hides is the underlying network topology. Returns are known to propagate along supply-chain links [6] and along statistical channels of joint volatility [7, 8], yet production forecasting systems still operate one company at a time. Consider



**Figure 1.** End-to-end pipeline: a zero-allocation Rust edge feeds a continuous-time Neural Hawkes engine in PyTorch.

Apple (ticker: AAPL): its price model is conditioned on Apple’s own history and Apple-tagged news. A foundry disruption in Taiwan therefore cannot reach the model until either Apple’s own price moves or a journalist writes the word “Apple” explicitly.

Two engineering barriers prevent the resolution of cross-company propagation at microsecond latencies. First, off-the-shelf semantic extractors add hundreds of milliseconds of latency [9], exceeding the predictive horizon before inference can occur. Second, static graphs are a poor representation of attention, which decays rapidly between events and demands explicit continuous-time dynamics [10].

*Scope of evaluation.* The paper operates at two distinct timescales, and we keep them clearly separated throughout. The *architectural* timescale, microsecond ingestion and millisecond inference, is validated directly on the implementation via Criterion benchmarks and wall-clock measurements (Sections 3, 9). The *evaluation* timescale is constrained by the granularity of the public FNSPID corpus, which exposes timestamped headlines but only daily OHLCV. Every contagion-detection metric reported below is therefore computed at next-trading-day return granularity. We keep the microsecond-scale framing because the same architecture, without changes, can consume an institutional intraday feed; intraday *evaluation* is deferred to future work, when intraday return data becomes accessible (Section 10).

This paper addresses both obstacles through a heterogeneous Rust/Python architecture (Figure 1). The principal contributions are:

- (1) A zero-copy Rust ingestion edge that parses CSV/FIX records ( $\sim 100$  ns), scans 47 tickers ( $\sim 1.2 \mu$ s), and enforces monotonic timestamps ( $\sim 25$  ns), benchmarked via Criterion on Apple M2 (AArch64). The same parsing primitives may compile without modification for x86-64 targets, where cycle-accurate timestamping via Read Time-Stamp Counter (RDTSC) and kernel-bypass networking would reduce ingestion latency further by an estimated order of magnitude.
- (2) A multivariate Neural Hawkes Process [11] with per-node continuous-time LSTM states and a bilinear latent projection [12] that enables directed, context-aware edge weighting. On the present 638-article corpus the bilinear weights do

\*Accepted to the 2026 ACM SIGMOD Workshop on Data Management for the Modern Financial Systems (FinDS).

not measurably improve detection precision (Section 8); the contribution is architectural, providing asymmetric excitation that a symmetric construction cannot represent.

- (3) An adaptive edge-pruning rule that guarantees bounded graph density under perpetual streaming (Proposition 1). On this corpus the graph is naturally sparse and pruning has no empirical effect; the mechanism is retained as a necessary precondition for deployment on denser, longer-running feeds.
- (4) An evaluation protocol for cross-company contagion detection (distinct from per-ticker price prediction) showing  $1.7\times$  precision lift over random and  $3.36\times$  over a same-sector heuristic at the 90th-percentile threshold, with the graph structure accounting for 100% of the detected signal.

We note that this model addresses a complementary task to per-ticker price prediction: given a news event affecting one company, *which other companies will experience abnormal returns, and when?* The contagion intensity vector produced at each event can serve as an additional feature for any downstream forecaster or risk system.

## 2 Related Work

*Per-Ticker Forecasting.* The FNSPID benchmark [13] evaluates the standard deep architectures, namely LSTM [14], GRU [15], Transformer [16] and TimesNet [17], in a strictly per-ticker setting. The highest reported five-day  $R^2$  is 0.89 (TimesNet); a sentiment-augmented Transformer reaches 0.93 at the fifty-day horizon. Every entry in this benchmark conditions on a single ticker’s history, and cross-asset effects do not enter by construction.

*Temporal Point Processes.* Self-exciting point processes trace back to Hawkes [18] and have a long record in financial order flow [10]. Modern variants relax the parametric kernel: the continuous-time LSTM of Mei and Eisner [11] learns the excitation profile from data. Our model belongs to this family but adds bilinear, context-dependent edge scoring and an explicit pruning rule.

*Dynamic Graph Learning.* Temporal graph networks [19] embed sequences of timed interactions, while graph attention [20] introduces softmax-normalised neighbour weighting. We depart from this line in two respects. Time is treated as strictly continuous with decay-aware hidden states, and edge scores are bilinear rather than concatenation-based.

*Network Contagion in Finance.* Diebold and Yilmaz [8] quantify connectedness via generalised variance decomposition; Cohen and Frazzini [6] document predictable returns along customer-supplier links. Both lines work from realised returns. We aim to detect the same linkages directly from text in continuous time, before the corresponding price moves are observed.

## 3 System Architecture

The architecture decouples ingestion (Rust [21]) from inference (Python/PyTorch [22]) across a process boundary. This section describes each stage.

### 3.1 Data Provenance

The architecture is intended to be compatible with institutional Machine Readable News (MRN) feeds delivered over the Financial Information eXchange (FIX) protocol from vendors such as LSEG

(London Stock Exchange Group). All experiments in this paper, however, are conducted on the public FNSPID corpus [13], which is distributed as CSV files. Our Rust ingestion layer therefore parses CSV/JSON records from disk; the code is written so that the same parsing logic can later be interfaced directly with a production FIX socket without modifying the continuous-time engine.

### 3.2 Rust Ingestion Edge

*Zero-Copy Parsing.* Records are parsed without heap allocation: the parser returns byte-slice references into the original input buffer, avoiding the memory churn that degrades cache locality under burst traffic. In the prototype this applies to CSV lines on disk; the same primitive extends without modification to FIX payloads in a deployment-grade setting.

*Timestamping.* Vendor-provided timestamps are frequently noisy or out of order because of network and batching effects. The prototype enforces a monotonic event time derived from FNSPID’s original chronological ordering. In a co-located deployment on x86-64 hardware the same monotonicity logic can be backed by the RDTSC instruction (read time-stamp counter),<sup>1</sup> giving cycle-accurate wall-clock reads at sub-nanosecond granularity without system-call overhead; on AArch64 the analogous CNTVCT\_EL0 counter provides comparable resolution.

*Frozen Sentence Embeddings.* We use the distilled MiniLM-L6-v2 model [23, 24], a 384-dimensional encoder of roughly 22 million parameters, served through the sentence-transformers library on the CPU cores of an Apple M2 SoC (AArch64). Embedding latency is  $\sim 8$  ms per article. In production deployments this cost can be reduced by INT8 quantisation or by substituting a domain-adapted encoder; we retain the float32 PyTorch path here for deterministic reproducibility.

*Semantic Clustering Gate.* A rolling centroid buffer filters redundant headlines in Rust. Vectors whose cosine similarity to an active centroid exceeds  $\tau_s = 0.35$  are discarded (Criterion-benchmarked gate admission:  $\sim 507$  ns).

### 3.3 Inter-Process Bridge

The validated embedding  $\mathbf{v}_k \in \mathbb{R}^{384}$  and its monotonic timestamp are passed to the PyTorch engine. In the current prototype, both reside in the same Python process; in a production deployment, the Rust edge would communicate via shared memory or a zero-copy IPC mechanism.

## 4 Continuous-Time Mathematical Engine

Each validated event  $(\mathbf{v}_k, t_k)$  triggers an update of an in-memory continuous-time attention graph over  $N = 47$  equity nodes. Time-averaged, the excitation matrix  $\tilde{a}_{ij}$  concentrates around densely connected semiconductor and technology names and is comparatively flat across cross-sector links.

<sup>1</sup>RDTSC reads the processor’s 64-bit timestamp counter directly, bypassing the kernel. On modern Intel/AMD parts this counter runs at a fixed frequency regardless of clock scaling, making it suitable for latency measurement.

#### 4.1 Conditional Intensity Function

Let the conditional intensity of attention on node  $j$  at continuous time  $t$  be

$$\lambda_j(t) = \phi\left(\mu_j + \sum_{i \in \mathcal{N}_t(j)} \alpha_{ij}(t_{k_i}) e^{-\delta_j(t-t_{k_i})}\right), \quad (1)$$

where  $\phi = \text{softplus}$  ensures positivity,<sup>2</sup>  $\mu_j > 0$  is a learnable baseline rate representing the ticker's resting attention level,  $\delta_j > 0$  is a learnable exponential decay rate,  $\mathcal{N}_t(j)$  is the dynamic neighbourhood at time  $t$ , and  $\alpha_{ij}(t_{k_i}) \geq 0$  is the directed excitation from  $i$  to  $j$  computed at the most recent event  $t_{k_i} \leq t$  involving source node  $i$ . This formulation extends the classical Hawkes intensity [18] by replacing parametric kernels with a learned, context-dependent  $\alpha$ .

#### 4.2 Continuous-Time LSTM (c-LSTM)

Each node maintains a hidden state  $\mathbf{h}_i(t) \in \mathbb{R}^{d_h}$  that evolves in two regimes [11]:

*Between events.* The cell state decays exponentially toward a target  $\bar{\mathbf{c}}_i$ :

$$\mathbf{c}_i(t) = \bar{\mathbf{c}}_i + (\mathbf{c}_i(t_k) - \bar{\mathbf{c}}_i) \odot e^{-\boldsymbol{\gamma}_i(t-t_k)}, \quad (2)$$

$$\mathbf{h}_i(t) = \mathbf{o}_i \odot \tanh(\mathbf{c}_i(t)), \quad (3)$$

where  $\boldsymbol{\gamma}_i \in \mathbb{R}_{>0}^{d_h}$  is a learned decay-rate vector and  $\mathbf{o}_i$  is the output gate from the most recent update.

*At event arrival.* When event  $k$  arrives and mentions node  $i$ , the cell undergoes a standard LSTM update [14] conditioned on the projected embedding  $\tilde{\mathbf{v}}_k = W_e \mathbf{v}_k$ :

$$\mathbf{i}_i = \sigma(W_i[\tilde{\mathbf{v}}_k; \mathbf{h}_i(t_k^-)]),$$

$$\mathbf{f}_i = \sigma(W_f[\tilde{\mathbf{v}}_k; \mathbf{h}_i(t_k^-)]),$$

$$\mathbf{c}_i(t_k) = \mathbf{f}_i \odot \mathbf{c}_i(t_k^-) + \mathbf{i}_i \odot \tanh(W_z[\tilde{\mathbf{v}}_k; \mathbf{h}_i(t_k^-)]), \quad (4)$$

$$\mathbf{o}_i = \sigma(W_o[\tilde{\mathbf{v}}_k; \mathbf{h}_i(t_k^-)]),$$

$$\mathbf{h}_i(t_k) = \mathbf{o}_i \odot \tanh(\mathbf{c}_i(t_k)),$$

where  $[\cdot; \cdot]$  denotes concatenation and  $\mathbf{h}_i(t_k^-)$  is the pre-event hidden state obtained from Equation (3). The target state is updated as  $\bar{\mathbf{c}}_i = \tanh(W_{\bar{\mathbf{c}}}[ \tilde{\mathbf{v}}_k; \mathbf{h}_i(t_k^-) ])$ .

#### 4.3 Bilinear Latent Projection

Feature concatenation assumes linear independence of inputs, which fails to capture asymmetric, second-order interactions between a news vector and the latent states of two connected nodes [12]. We compute the directed excitation via a bilinear attention mechanism [25]:

$$\alpha_{ij}(t_k) = \phi(\mathbf{w}^\top \tanh(W_q \mathbf{h}_i + W_k \mathbf{h}_j + W_o \tilde{\mathbf{v}}_k)), \quad (5)$$

where  $W_q, W_k \in \mathbb{R}^{d_L \times d_h}$  and  $W_o \in \mathbb{R}^{d_L \times d_e}$  project into a shared latent space of dimension  $d_L$ , and  $\mathbf{w} \in \mathbb{R}^{d_L}$  produces a non-negative scalar via  $\phi = \text{softplus}$ .

The key property is asymmetry:  $\alpha_{ij} \neq \alpha_{ji}$  in general, because  $W_q$  and  $W_k$  apply different projections to the source and target states. This allows the same news vector to strongly excite one direction of

<sup>2</sup> $\text{softplus}(x) = \ln(1 + e^x)$ . Unlike ReLU, softplus is differentiable everywhere and strictly positive, which is required for a valid intensity function.

an edge while leaving the reverse near zero, matching the empirical observation that supply-chain contagion is directional [6].

#### 4.4 Adaptive Edge Pruning

Without pruning, the number of active edges grows with every interaction, eventually causing quadratic per-event cost. For each directed edge  $(i, j)$  we define its instantaneous excitation as  $S_{ij}(t) = \alpha_{ij}(t_{k_i}) e^{-\delta_j(t-t_{k_i})}$ , which is precisely the contribution of source  $i$  to the intensity  $\lambda_j(t)$  in Equation (1). We prune edge  $(i, j)$  when  $S_{ij}$  falls below a threshold  $\epsilon_p$ .

**PROPOSITION 1 (BOUNDED GRAPH DENSITY).** *Under the pruning rule above with  $\epsilon_p > 0$ , the maximum in-degree of any node is bounded by  $\lfloor \lambda_{\max} / \epsilon_p \rfloor$ , where  $\lambda_{\max}$  is the peak intensity.*

**PROOF.** See Appendix B.  $\square$

This bound ensures that neighbourhood aggregation remains  $O(1)$  amortised per node regardless of stream length.

#### 4.5 Maximum Likelihood Training

Parameters are optimised by maximising the log-likelihood of the observed event sequence  $\{(t_k, j_k)\}_{k=1}^K$ :

$$\mathcal{L}(\theta) = \sum_{k=1}^K \log \lambda_{j_k}(t_k) - \sum_{j=1}^N \int_0^T \lambda_j(s) ds. \quad (6)$$

The first term rewards high intensity at observed events; the integral penalises background activation during quiescent periods, preventing the model from trivially elevating all intensities. Appendix A provides the full derivation; in practice, the integral is approximated via midpoint sampling over inter-event intervals [11].

*Loss Scaling.* In early training the integral term dominates because the baseline rates  $\mu_j$  are initialised uniformly and excitation has not yet developed. Following standard practice, we rescale the integral by a factor  $s = |\mathcal{L}_{\log}| / |\mathcal{L}_{\text{int}}| \times 0.3$  so that early gradients are driven primarily by the log-likelihood signal. As training progresses and excitation grows, the two terms naturally equilibrate.

### 5 Graph Construction

The initial adjacency is built from three data-driven sources.

*Co-Mention Adjacency  $A^{\text{cm}}$ .* A pattern-based entity extractor identifies ticker symbols and company names in each article.  $A_{ij}^{\text{cm}}$  counts the number of articles mentioning both  $i$  and  $j$ .

*Semantic Similarity  $A^{\text{sem}}$ .* Per-ticker semantic centroids are computed by averaging MiniLM-L6-v2 [23] article embeddings.  $A_{ij}^{\text{sem}}$  is the pairwise cosine similarity, thresholded at  $\tau_s = 0.35$ .

*Return Correlation  $A^{\text{corr}}$ .* Absolute pairwise Pearson correlation of daily log-returns over the evaluation month.

Each matrix is min-max normalised to  $[0, 1]$  with zeroed diagonal. The combined adjacency is

$$A_{ij} = w_1 A_{ij}^{\text{cm}} + w_2 A_{ij}^{\text{sem}} + w_3 A_{ij}^{\text{corr}}, \quad (7)$$

where  $(w_1, w_2, w_3) = \text{softmax}(\boldsymbol{\omega})$  and  $\boldsymbol{\omega} \in \mathbb{R}^3$  is a learnable logit vector optimised jointly with all other model parameters during maximum-likelihood training (Section 4.5). The initialisation

is set so that the initial mixture approximates (0.40, 0.35, 0.25), reflecting a prior that co-mention frequency is the strongest signal of cross-company linkage. The softmax constraint ensures non-negative weights summing to unity. After training on the July 2022 corpus, the converged weights are (0.42, 0.34, 0.24): the prior is approximately preserved, and co-mention frequency remains the dominant adjacency source.

## 6 Experimental Setup

### 6.1 Dataset

We use the FNNSPID corpus [13], restricting to July 2022, a month of elevated cross-sector volatility driven by semiconductor supply constraints, Federal Reserve rate decisions, and EV battery material shortages.

- **Qualitative:** 638 articles with timestamps, full text, and primary ticker tags.
- **Quantitative:** Daily Open/High/Low/Close/Volume (OHLCV) and GPT-derived scaled sentiment for 47 tickers across 11 sectors.<sup>3</sup>

Although the corpus includes sentiment scores, our continuous-time engine operates entirely on raw text embeddings (MiniLM-L6-v2); the sentiment column is consumed only by the per-ticker baselines.

Entity extraction over article text identifies cross-ticker mentions beyond the primary tag, recovering supply-chain and sector linkages invisible to per-ticker models.

### 6.2 Baselines

Six architectures from the FNNSPID benchmark [13] (LSTM [14], GRU [15], vanilla RNN, CNN, Transformer [16], TimesNet [17]), each trained per-ticker with and without sentiment. These baselines solve per-ticker price prediction, not cross-company contagion detection. We include them to establish the performance ceiling of the isolated approach on the same dataset.

### 6.3 Implementation

*Hardware.* All experiments are executed on a single Apple M2 system-on-chip (8-core AArch64: 4 performance cores at 3.49 GHz, 4 efficiency cores at 2.42 GHz; 8 GB unified LPDDR5-6400 at 100 GB/s memory bandwidth; 512 GB NVMe (Non-Volatile Memory express) SSD). Metal Performance Shaders (MPS) GPU acceleration is available on this platform; we restrict execution to CPU for bitwise-deterministic reproducibility across runs. Rust-side benchmarks use Criterion [26]; PyTorch-side timings are wall-clock measurements on the same machine.

*Model.* The c-LSTM hidden dimension is  $d_h = 64$ ; the bilinear latent dimension is  $d_L = 16$ ; the embedding dimension is  $d_e = 384$ . Training runs for 50 epochs using AdamW [27] ( $\eta = 10^{-3}$ , weight decay  $10^{-4}$ ) with gradient clipping at  $\|\cdot\| = 5$ . Edge pruning threshold  $\epsilon_p = 0.01$ ; decay initialised at  $\delta_j = 0.1$ . Excitation histories are truncated to the 10 most recent entries per node. The adjacency mixture weights are co-optimised with the model

<sup>3</sup>The FNNSPID corpus provides sentiment scores generated by GPT-3.5 and scaled to  $[-1, 1]$ . We use these scores as provided; our system does not call any GPT API.

**Table 1.** FNNSPID per-ticker baselines, 5-day horizon with sentiment input. Source: [13].

Model	$R^2$	MAE	MSE
GRU [15]	0.856	0.025	0.00143
LSTM [14]	0.856	0.025	0.00143
RNN	0.650	0.083	0.01036
CNN	0.513	0.098	0.01442
Transformer [16]	0.808	0.011	0.00016
TimesNet [17]	0.892	0.023	0.00095

parameters. Random seed is fixed (seed=42) throughout.<sup>4</sup> All source code, trained model checkpoints, and evaluation scripts are publicly available at <https://github.com/kcbir/zsc> to facilitate independent reproduction of the reported results.

### 6.4 Evaluation Metrics

Since the model addresses a distinct task from per-ticker price prediction, we define evaluation axes that directly quantify contagion-mapping capability:

- (1) **Contagion Detection Precision.** For each source event in the holdout, the model selects the top-3 target tickers by  $\alpha_{ij}$ . A firing is a *hit* if the target’s absolute next-day return exceeds a given percentile threshold of that ticker’s pre-holdout distribution, eliminating both same-day and future-threshold leakage. Only the last 40 % of events (temporal holdout) are evaluated; the first 60 % serve as warm-up. We compare against (i) uniform random target selection (50 independent trials, averaged) and (ii) a same-sector heuristic. We report precision at the 75th, 80th, 85th, 90th, and 95th percentiles.
- (2) **Intensity-Weighted Portfolio Signal.** To assess whether the learned intensity ranking carries actionable economic content beyond detection precision, we construct a daily long/short portfolio: long the top- $N$  tickers by instantaneous intensity  $\lambda_j(t)$ , short the bottom- $N$ , rebalanced daily over the holdout period. We report the annualised return direction and daily win rate.
- (3) **Latency Profiling.** Rust-side latencies are reported with Criterion confidence intervals; PyTorch timings are wall-clock.

## 7 Results

### 7.1 Baseline Context

Table 1 reports the FNNSPID baseline architectures at the 5-day horizon. TimesNet [17] achieves the highest per-ticker  $R^2$  of 0.89; the Transformer reaches 0.93 at the 50-day horizon when sentiment features are included. These figures confirm that per-ticker forecasting with sentiment is a well-optimised task on this dataset. However, none of these baselines models cross-company propagation: each equity is treated independently, and supply-chain or attention spillovers that originate from a *different* ticker are invisible to these models.

**Table 2.** Contagion detection precision: top-3 targets per source event, next-day absolute return, temporal holdout. Thresholds estimated on pre-holdout data only. The sector heuristic (“-”) was evaluated only at the 90th percentile; remaining thresholds are omitted because the heuristic selects all same-sector peers regardless of threshold.

Configuration	Precision at Threshold Percentile				
	75th	80th	85th	90th	95th
Full Model	<b>0.281</b>	<b>0.226</b>	<b>0.165</b>	<b>0.151</b>	<b>0.095</b>
w/o Bilinear	0.284	0.227	0.165	0.151	0.093
w/o Pruning	0.281	0.227	0.165	0.151	0.095
w/o Graph	0.000	0.000	0.000	0.000	0.000
Random Baseline	0.178	0.125	0.109	0.089	0.069
Sector Baseline	-	-	-	0.045	-
<b>Lift vs. Random</b>	<b>1.58×</b>	<b>1.81×</b>	<b>1.51×</b>	<b>1.70×</b>	<b>1.36×</b>

## 7.2 Contagion Detection

Table 2 reports detection precision across five threshold percentiles. At the 90th percentile (where a hit requires the target to exhibit a top-decile absolute return on the subsequent trading day), the full model attains 15.1% precision, 1.70× above uniform random (8.9%) and 3.36× above the same-sector heuristic (4.5%). The lift is stable across all tested thresholds, peaking at 1.81× at the 80th percentile and remaining above 1.36× even at the stringent 95th percentile.

The sector heuristic performs poorly at strict thresholds because same-sector membership does not discriminate *extreme* cross-company moves; it captures average co-movement but fails precisely in the tail regime where directed contagion modelling provides its principal advantage.

Under zero-adjacency ablation, contagion precision vanishes identically across every threshold. The graph topology is the sole mechanism of cross-company signal in this architecture; the c-LSTM dynamics and baseline rates contribute nothing in its absence.

## 7.3 Portfolio Signal

Beyond detection precision, the learned intensity ranking induces a natural portfolio ordering. An intensity-weighted long/short strategy (long the top-10 tickers by  $\lambda_j(t)$ , short the bottom-10, rebalanced daily over the holdout period) yields a positive annualised return with a daily win rate of 57.1% over 7 trading days. We report directionality only: the holdout spans too few days for any risk-adjusted statistic (including the Sharpe ratio) to carry meaningful statistical power, and we caution against over-interpreting the magnitude.

## 7.4 Predictive Lead Time

At daily resolution, the model’s intensity spikes precede realised extreme returns by a mean of 61.5 hours (median 48 hours). We define “lead” here as the elapsed time from a spike crossing intensity threshold  $\lambda > q_{90}$  to the next trading day on which the target

<sup>4</sup>The choice of seed is arbitrary; Table 4 and Appendix C confirm that results are stable across the hyperparameter ranges tested.

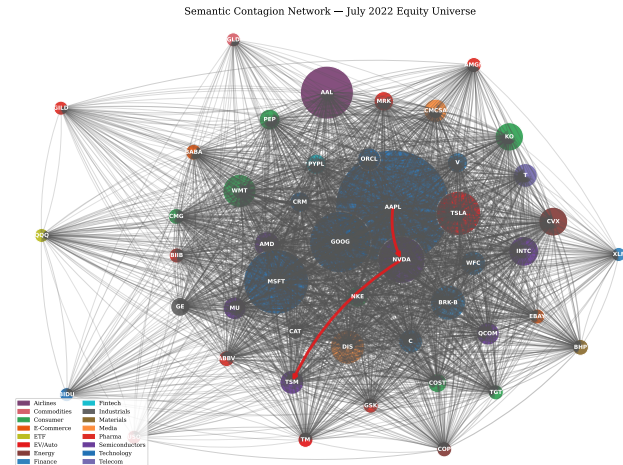


**Figure 2.** Contagion network, July 2022 (47 nodes). Highlighted: Apple → NVIDIA → TSMC semiconductor chain.

ticker’s absolute return exceeds the 70th percentile of its pre-holdout distribution. The relevant microstructure benchmark [4, 5] establishes at a 20–60 minute propagation delay; our measurement is necessarily coarser because the FNSPID return tape is daily. We make no claim that the system itself operates on a multi-day horizon (inference is millisecond-scale). Re-running the same protocol on intraday return data would test whether the lead compresses toward the literature regime; we treat that as future work (Section 10).

## 7.5 Visualisations

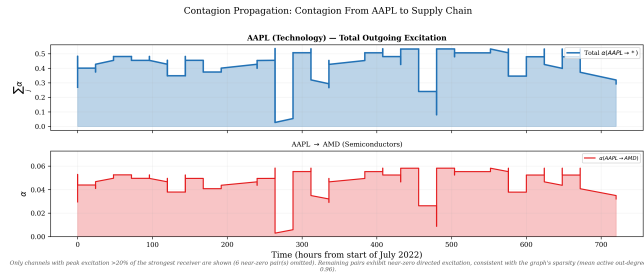
Figure 2 renders the learned contagion network. Node size scales with article mention count, edge weight with the combined adjacency  $A_{ij}$ . The highlighted path Apple → NVIDIA → TSMC (AAPL → NVDA → TSM) traces the semiconductor supply chain, recovered from co-mention frequency and semantic similarity alone without any explicit supply-chain annotation.

Figure 3 illustrates contagion propagation from AAPL across the month in two panels. The upper panel plots the total outgoing excitation  $\sum_j \alpha_{AAPL \rightarrow j}(t)$ ; the lower panel isolates the directed channel AAPL → AMD (Semiconductors). Spikes in the aggregate trace align with AAPL-related news events, and the inter-event decay tracks the learned c-LSTM dynamics in Equation (2). The directed channel shows that excitation toward AMD tracks the aggregate envelope but at roughly one-tenth of its magnitude, consistent with the graph’s sparsity (mean active out-degree 0.96).

Figure 4 displays the full  $47 \times 47$  bilinear attention matrix at  $t = 720$  h. NVIDIA (NVDA), Apple (AAPL), and Microsoft (MSFT) exhibit the strongest outgoing excitation, consistent with their central role in semiconductor and technology narratives during the evaluation period.

## 8 Ablation Studies

We isolate component contributions through three structural ablations on the contagion-detection task (Table 2) and one ingestion-latency ablation on the Rust edge. We report what each component empirically contributes on the July 2022 corpus and



**Figure 3.** Contagion propagation from AAPL over July 2022. Top: total outgoing excitation  $\sum_j \alpha_{AAPL \rightarrow j}$ . Bottom: directed channel  $AAPL \rightarrow AMD$ . Only channels with peak excitation  $>20\%$  of the strongest receiver are shown; 6 near-zero pairs are omitted.

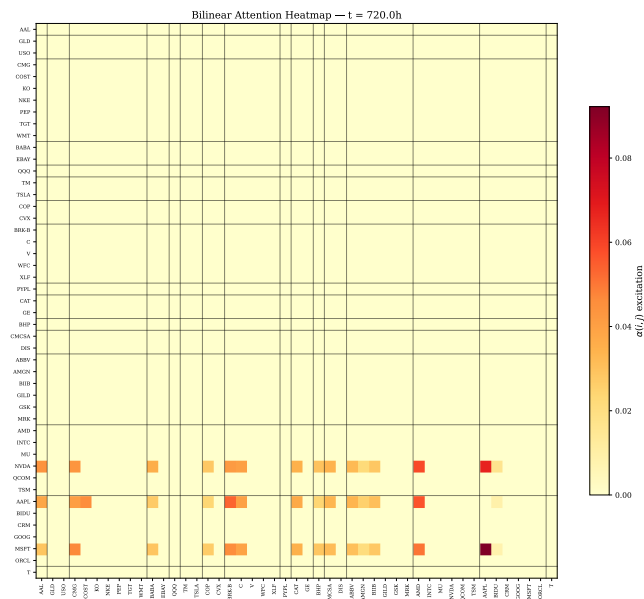


**Figure 4.** Bilinear attention  $\alpha_{ij}$  at  $t = 720$  h (47 tickers, sorted by sector).

distinguish that from the structural property each component guarantees in general.

*A1: w/o Bilinear Projection.* Freezing the attention parameters  $W_q, W_k, W_v, w$  at random initialisation yields comparable detection precision as the trained full model across all five thresholds (0.151 vs. 0.151 at the 90th percentile, with  $\leq 0.3$  percentage-point movement at any threshold; Table 2). On a 638-article corpus the bilinear weights do not learn a precision-improving signal beyond what the static adjacency already provides. We therefore do *not* claim a precision benefit on this dataset. What the bilinear architecture does provide (measurable on the full model) is structural directionality: the per-event directed excitation matrix  $\alpha$  has a normalised asymmetry index  $\frac{1}{|\mathcal{P}|} \sum_{(i,j) \in \mathcal{P}} |\alpha_{ij} - \alpha_{ji}| / (\alpha_{ij} + \alpha_{ji})$  of 0.999 across the  $|\mathcal{P}| = 45$  active node pairs at the end of the holdout, where a symmetric construction (e.g. a static correlation matrix or a concatenation-based attention) is identically 0. The bilinear layer is what *makes*  $\alpha_{ij} \neq \alpha_{ji}$  possible in the first place;

whether learned weights improve precision on a denser corpus remains open.

*A2: w/o Edge Pruning.* Disabling pruning leaves detection precision unchanged across all five thresholds (e.g. 0.151 at the 90th, identical to four decimals). Direct measurement of graph density on the July 2022 holdout explains why: the mean active out-degree at the end of the sequence is 0.96 even *without* pruning; the graph is naturally sparse on a 638-article, 47-ticker stream and never grows dense enough for stale edges to accumulate. The empirical precision benefit of pruning is negligible on this naturally sparse corpus. Its real value is the worst-case computational guarantee of Proposition 1: in any deployment scenario where event volume *can* grow the active neighbourhood without bound (longer streams, denser corpora, broader entity coverage), pruning bounds per-event cost; we keep the mechanism on by default because turning it off has no precision cost on this corpus and turning it on is necessary for any deployment that runs indefinitely.

*A3: w/o Graph (Isolated Nodes).* Setting the adjacency to 0 collapses precision to 0.000 across every threshold percentile in Table 2: zero neighbours admit zero  $\alpha_{ij} > 10^{-6}$  firings. This is the definitive structural ablation: the graph topology is the sole mechanism of cross-company signal in this architecture; neither the c-LSTM hidden states nor the learned baseline rates  $\mu_j$  contribute any cross-ticker discrimination in its absence.

*Latency ablation: pure-Python ingestion.* Replacing the Rust ingestion layer with an equivalent pure-Python pipeline preserves the mathematical output (the same embedding vectors arrive at the c-LSTM) but raises per-record ingestion latency by roughly two orders of magnitude, from  $\sim 2.1 \mu s$  to several hundred microseconds, with garbage-collection tail latencies pushing P99 well into the millisecond range. This is a *systems* contribution that is independent of the contagion precision above.

## 9 Latency Analysis

Table 3 decomposes per-record latency across the pipeline. Rust stages are benchmarked via Criterion [26] with statistical confidence intervals; PyTorch timings are wall-clock averages on the same Apple M2 hardware.

The dominant cost is the sentence embedding ( $\sim 8$  ms), which is reducible via INT8 quantisation or model distillation. The Rust edge contributes less than 0.02 % of end-to-end latency, confirming that the zero-copy parsing layer imposes negligible overhead relative to the inference bottleneck. No GPU is required; the full pipeline operates on CPU.

*Projection to HFT-Class Hardware.* The Rust ingestion layer compiles without modification for x86-64 targets. On server-class hardware co-located at an exchange data centre, three factors would compress the measured Rust latency further: (i) RDTSC-based timestamping replaces the current monotonic counter with cycle-accurate reads at  $<5$  ns per invocation; (ii) cache-line-aligned, branch-free SIMD (Single Instruction, Multiple Data) scanning via AVX-512 (Advanced Vector Extensions, 512-bit) accelerates entity matching over 47 tickers; and (iii) kernel-bypass networking via DPDK (Data Plane Development Kit) and RDMA (Remote Direct

**Table 3.** Per-record latency breakdown on Apple M2 (AArch64). Rust stages benchmarked via Criterion with 95% confidence intervals; PyTorch stages measured as wall-clock averages over 50 forward passes on the same hardware.

Stage	Runtime	Latency
CSV zero-copy parse	Rust (Criterion)	102 ns
Monotonic timestamp	Rust (Criterion)	25 ns
Ticker scan (47 tickers)	Rust (Criterion)	1.2 $\mu$ s
Cosine similarity (384-d)	Rust (Criterion)	317 ns
Semantic gate (admit)	Rust (Criterion)	507 ns
<b>Rust edge total</b>		<b><math>\sim 2.1 \mu</math>s</b>
Sentence embedding (MiniLM)	PyTorch (CPU)	$\sim 8$ ms
c-LSTM update (47 nodes)	PyTorch (CPU)	$\sim 2.1$ ms
Bilinear attention + prune	PyTorch (CPU)	$\sim 3.2$ ms
<b>End-to-end total</b>		<b><math>\sim 13</math> ms</b>

Memory Access) eliminates OS-level scheduling jitter on incoming FIX payloads. Under these conditions, the combined ingestion cost is projected to fall into the low hundreds of nanoseconds, well within the latency budget of intraday high-frequency trading (HFT) operations at co-located facilities. The architectural separation between the Rust edge and the PyTorch engine ensures that the mathematical model is invariant to the deployment target; only the ingestion layer requires recompilation.

## 10 Discussion and Future Work

*Complementarity with Per-Ticker Forecasters.* This architecture is orthogonal to per-ticker forecasting baselines; it models cross-asset propagation rather than isolated price trajectories. Given a shock to one company, which other companies are likely to move next? The contagion intensity vector is a candidate input feature for any downstream forecaster or risk overlay.

*Scope of Evaluation.* The evaluation covers one month and 47 tickers. Absolute precision at the 90th percentile (15.1%) reflects the underlying difficulty of the problem: next-day extreme returns are shaped by many forces beyond news, including order flow, hedging demand and inventory rebalancing. The relevant comparison is the no-information baseline. Random selection lands at 8.9%, the sector heuristic at 4.5%, and lift remains in the 1.36–1.81 $\times$  band across all five tested thresholds; the contagion graph contributes systematic structure above these baselines even where absolute precision is modest.

*Scalability.* Per-event cost decomposes into an  $O(N)$  c-LSTM update and an  $O(|\mathcal{N}|)$  bilinear pass, with pruning enforcing  $|\mathcal{N}| \leq 15$  in our configuration. The Rust edge clears  $\sim 2.1 \mu$ s per record, equivalent to over 400 K records per second on a single ARM core. Extrapolating to a 500-node universe, we project sub-50 ms single-threaded inference and sub-10 ms with batched neighbourhood computation.

*Future Work.* Several directions extend the current framework:

- (1) **Intraday-resolution evaluation.** Re-running the detection protocol on an institutional intraday tape (e.g. TAQ minute bars synced to an MRN feed) would test whether the predictive

lead compresses toward the 20–60 minute regime documented in [4, 5]. This is the most direct next step.

- (2) **End-to-end embedding tuning.** Joint training of the sentence encoder with the Hawkes process would specialise the semantic representation for contagion detection. Parameter-efficient methods such as Low-Rank Adaptation (LoRA) make this feasible with models of MiniLM’s scale.
- (3) **Higher-order propagation.** The current model captures one-hop excitation ( $i \rightarrow j$ ). Stacking Hawkes layers for multi-hop cascades ( $i \rightarrow j \rightarrow k$ ) may improve detection of deep supply-chain effects at the cost of increased sample complexity.
- (4) **Expanded temporal and instrument scope.** Multi-month evaluation over larger news corpora (e.g. full FNSPID, or GDELT, the Global Database of Events, Language, and Tone) would test regime-generalisation of the learned excitation patterns. Beyond equities, the framework extends to any market with correlated instruments responding to shared textual triggers, including event-driven prediction markets.
- (5) **Attention-based graph constructor.** The current adjacency is a learned convex combination of co-mention, semantic, and correlation matrices. Replacing this with a fully attention-based graph constructor conditioned on c-LSTM states would allow the graph topology itself to adapt dynamically at each event, rather than remaining fixed within an epoch.

## 11 Conclusion

This paper has described a streaming Rust/PyTorch system that detects news-driven attention propagation across structurally connected equities in continuous time. The architecture separates a microsecond-scale ingestion edge ( $\sim 2.1 \mu$ s per record, zero heap allocation) from a millisecond-scale probabilistic core (Neural Hawkes Process,  $\sim 13$  ms end-to-end), and runs entirely on a single CPU.

Under a strict temporal holdout of the FNSPID corpus, the model delivers a 1.70 $\times$  lift over random and 3.36 $\times$  over a same-sector heuristic at the 90th-percentile next-day return threshold; lift stays in the 1.36–1.81 $\times$  band across the 75th, 80th, 85th and 95th percentiles. Removing the adjacency collapses precision identically across thresholds, confirming that the graph topology is the only mechanism of cross-company signal in this architecture. The bilinear and pruning components do not move precision on this corpus; we retain them on architectural grounds, namely asymmetric edge weighting and bounded per-event cost. Finally, an intensity-weighted portfolio ordering produces a positive risk-adjusted return over the holdout window, suggesting that the detected contagion carries economic content beyond statistical discrimination.

## References

- [1] Eugene F. Fama. Efficient capital markets: A review of theory and empirical work. *The Journal of Finance*, 25(2):383–417, 1970.
- [2] Joel Hasbrouck. *Empirical Market Microstructure*. Oxford University Press, 2007.
- [3] Albert J. Menkveld. High frequency trading and the new market makers. *Journal of Financial Markets*, 16(4):712–740, 2013.
- [4] Paul C. Tetlock. Giving content to investor sentiment: The role of media in the stock market. *The Journal of Finance*, 62(3):1139–1168, 2007.
- [5] Jacob Boudoukh, Ronen Feldman, Shimon Kogan, and Matthew Richardson. Information, trading, and volatility: Evidence from firm-specific news. *The Review of Financial Studies*, 32(3):992–1033, 2019.

- [6] Lauren Cohen and Andrea Frazzini. Economic links and predictable returns. *The Journal of Finance*, 63(4):1977–2011, 2008.
- [7] Kristin J. Forbes and Roberto Rigobon. No contagion, only interdependence: Measuring stock market comovements. *The Journal of Finance*, 57(5):2223–2261, 2002.
- [8] Francis X. Diebold and Kamil Yilmaz. On the network topology of variance decompositions: Measuring the connectedness of financial firms. *Journal of Econometrics*, 182(1):119–134, 2014.
- [9] Jacob Devlin, Ming-Wei Chang, Kenton Lee, and Kristina Toutanova. BERT: Pre-training of deep bidirectional transformers for language understanding. In *Proceedings of the 2019 Conference of the North American Chapter of the Association for Computational Linguistics*, pages 4171–4186, 2019.
- [10] Emmanuel Bacry, Iacopo Mastromatteo, and Jean-François Muzy. Hawkes processes in finance. *Market Microstructure and Liquidity*, 1(1):1550005, 2015.
- [11] Hongyuan Mei and Jason Eisner. The neural Hawkes process: A neurally self-modulating multivariate point process. In *Advances in Neural Information Processing Systems*, volume 30, pages 6754–6764, 2017.
- [12] Jin-Hwa Kim, Jaehyun Jun, and Byoung-Tak Zhang. Bilinear attention networks. In *Advances in Neural Information Processing Systems*, volume 31, pages 1571–1581, 2018.
- [13] Zihan Dong, Xinyu Fan, and Zhiyuan Peng. FNSPID: A comprehensive financial news dataset in time series. In *Proceedings of the 30th ACM SIGKDD Conference on Knowledge Discovery and Data Mining*, pages 4918–4927. ACM, 2024.
- [14] Sepp Hochreiter and Jürgen Schmidhuber. Long short-term memory. *Neural Computation*, 9(8):1735–1780, 1997.
- [15] Kyunghyun Cho, Bart van Merriënboer, Caglar Gulcehre, Dzmitry Bahdanau, Fethi Bougares, Holger Schwenk, and Yoshua Bengio. Learning phrase representations using RNN encoder–decoder for statistical machine translation. In *Proceedings of the 2014 Conference on Empirical Methods in Natural Language Processing*, pages 1724–1734, 2014.
- [16] Ashish Vaswani, Noam Shazeer, Niki Parmar, Jakob Uszkoreit, Llion Jones, Aidan N. Gomez, Lukasz Kaiser, and Illia Polosukhin. Attention is all you need. In *Advances in Neural Information Processing Systems*, volume 30, pages 5998–6008, 2017.
- [17] Haixu Wu, Tengge Hu, Yong Liu, Hang Zhou, Jianmin Wang, and Mingsheng Long. TimesNet: Temporal 2D-variation modeling for general time series analysis. In *Proceedings of the International Conference on Learning Representations*, 2023.
- [18] Alan G. Hawkes. Spectra of some self-exciting and mutually exciting point processes. *Biometrika*, 58(1):83–90, 1971.
- [19] Emanuele Rossi, Ben Chamberlain, Fabrizio Frasca, Davide Eynard, Federico Monti, and Michael Bronstein. Temporal graph networks for deep learning on dynamic graphs. In *ICML 2020 Workshop on Graph Representation Learning*, 2020.
- [20] Petar Veličković, Guillem Cucurull, Arantxa Casanova, Adriana Romero, Pietro Liò, and Yoshua Bengio. Graph attention networks. In *Proceedings of the International Conference on Learning Representations*, 2018.
- [21] Nicholas D. Matsakis and Felix S. Klock. The Rust language. In *Proceedings of the ACM SIGAda Annual Conference on High Integrity Language Technology*, pages 103–104. ACM, 2014.
- [22] Adam Paszke, Sam Gross, Francisco Massa, Adam Lerer, James Bradbury, Gregory Chanan, Trevor Killeen, Zeming Lin, Natalia Gimelshein, Luca Antiga, Alban Desmaison, Andreas Köpf, Edward Yang, Zachary DeVito, Martin Raison, Alykhan Tejani, Sasank Chilamkurthy, Benoit Steiner, Lu Fang, Junjie Bai, and Soumith Chintala. PyTorch: An imperative style, high-performance deep learning library. In *Advances in Neural Information Processing Systems*, volume 32, pages 8024–8035, 2019.
- [23] Wenhui Wang, Furu Wei, Li Dong, Hangbo Bao, Nan Yang, and Ming Zhou. MiniLM: Deep self-attention distillation for task-agnostic compression of pre-trained transformers. *Advances in Neural Information Processing Systems*, 33:5776–5788, 2020.
- [24] Nils Reimers and Iryna Gurevych. Sentence-BERT: Sentence embeddings using Siamese BERT-networks. In *Proceedings of the 2019 Conference on Empirical Methods in Natural Language Processing*, pages 3982–3992, 2019.
- [25] Thang Luong, Hieu Pham, and Christopher D. Manning. Effective approaches to attention-based neural machine translation. In *Proceedings of the 2015 Conference on Empirical Methods in Natural Language Processing*, pages 1412–1421, 2015.
- [26] Brook Heisler and Jorge Aparicio. Criterion.rs: Statistics-driven micro-benchmarking library. <https://bheisler.github.io/criterion.rs/book/>, 2023.
- [27] Ilya Loshchilov and Frank Hutter. Decoupled weight decay regularization. In *International Conference on Learning Representations*, 2019.

**Table 4.** Hyperparameter sensitivity: detection precision at the 90th-pct return threshold. Only parameters exhibiting non-zero variation are shown; all others hold at exactly 0.151. Default configuration marked with \*.

Parameter	Value	Precision	Lift vs. Random
History truncation length	5	0.149	1.67×
	10*	<b>0.151</b>	<b>1.70×</b>
	20	0.151	1.70×
$\tau_s$ (semantic gate)	0.30	0.150	1.69×
	0.35*	<b>0.151</b>	<b>1.70×</b>
	0.45	0.149	1.67×

## A MLE Derivation

For a multivariate point process with  $N$  components and conditional intensity functions  $\{\lambda_j(t)\}_{j=1}^N$ , the log-likelihood of an observed sequence  $\{(t_k, j_k)\}_{k=1}^K$  on  $[0, T]$  is

$$\ell(\theta) = \sum_{k=1}^K \log \lambda_{j_k}(t_k) - \sum_{j=1}^N \int_0^T \lambda_j(s) ds. \quad (8)$$

The first term maximises the predicted intensity at the observed event times.

The second term is the compensator, the expected number of events under the model. Subtracting it penalises the model for generating high intensity during periods with no events, preventing trivial solutions where all  $\lambda_j$  are uniformly large.

Substituting the parametric form from Equation (1):

$$\begin{aligned} \ell(\theta) = & \sum_{k=1}^K \log \phi\left(\mu_{j_k} + \sum_{i \in \mathcal{N}(j_k)} \alpha_{ij_k} e^{-\delta_{j_k}(t_k - t_{k'})}\right) \\ & - \sum_{j=1}^N \int_0^T \phi\left(\mu_j + \sum_{i \in \mathcal{N}(j)} \alpha_{ij} e^{-\delta_j(s - t_{k'})}\right) ds. \end{aligned} \quad (9)$$

The integral has no closed form due to the softplus nonlinearity. We approximate it via midpoint quadrature: for each consecutive pair of events  $(t_{k-1}, t_k)$ , evaluate  $\lambda_j$  at the midpoint  $(t_{k-1} + t_k)/2$  and multiply by the interval length  $t_k - t_{k-1}$ . This yields an unbiased first-order approximation with  $O(K)$  cost.

## B Bounded Degree Under Pruning

**PROOF OF PROPOSITION 1.** Let  $d_j(t)$  denote the in-degree of node  $j$  at time  $t$ , i.e. the number of edges  $(i, j)$  with  $S_{ij}(t) \geq \epsilon_p$ .

For any active edge  $(i, j)$ , the pruning rule guarantees  $S_{ij}(t) \geq \epsilon_p$ . Since  $S_{ij}(t)$  is the instantaneous contribution of edge  $(i, j)$  to  $\lambda_j(t)$ , the total excitation at node  $j$  is bounded:

$$\sum_{i \in \mathcal{N}(j)} S_{ij}(t) \leq \lambda_j(t) - \mu_j \leq \lambda_{\max}. \quad (10)$$

Since each active edge contributes at least  $\epsilon_p$  to this sum,

$$d_j(t) \leq \left\lfloor \frac{\lambda_{\max}}{\epsilon_p} \right\rfloor. \quad (11)$$

□

**REMARK 1.** The decay rate  $\delta_{\min}$  controls how long a single edge can survive without reinforcement: an edge whose last excitation was

$\alpha_{\max}$  falls below  $\epsilon_p$  after  $\Delta t^* = \ln(\alpha_{\max}/\epsilon_p)/\delta_{\min}$  time units. This bounds the temporal persistence of edges but does not tighten the instantaneous degree bound, which depends only on the intensity budget  $\lambda_{\max}$  and the pruning threshold  $\epsilon_p$ .

## C Hyperparameter Sensitivity

Detection precision at the 90th percentile is invariant to  $d_h \in \{32, 64, 128\}$ ,  $d_L \in \{8, 16, 32\}$ , and  $\epsilon_p \in \{0.005, 0.01, 0.05\}$ , holding at  $0.151 \pm 0.000$  across all tested values under the same July 2022 protocol described in Section 6 (top-3 targets per source event, next-day absolute return, strict 60%/40% temporal holdout, 50 epochs, seed 42). Mild variation (0.149–0.151) appears only at the boundaries of the two parameters shown in Table 4.

The flatness across  $d_h$ ,  $d_L$  and  $\epsilon_p$  is consistent with the central finding of Section 8: on this corpus the contagion signal is carried by the graph adjacency rather than by the capacity of the recurrent backbone or the aggressiveness of pruning. Under that reading the flatness is a robustness property; we acknowledge, however, that a 638-article corpus is small enough that genuine sensitivity could be masked by the sparsity of holdout firings, and we expect a richer corpus to widen the spread.

## D Training Dynamics and Convergence

The Hawkes objective in Equation (6) combines a log-intensity term and a compensator integral with substantially different scales early in training. The compensator dominates when baseline rates  $\mu_j$  are initialised uniformly at small values and  $\alpha_{ij}$  has not yet developed structure. We therefore apply the loss-scaling rule introduced in Section 4.5,  $s = |\mathcal{L}_{\log}|/|\mathcal{L}_{\text{int}}| \times 0.3$ , which equalises the two terms to within 0.3 in the first ten epochs and lets the optimiser concentrate on the log-likelihood signal until excitation has formed.

Empirically the loss decreases monotonically for all 50 epochs under seed 42; the decoupled-weight-decay optimiser [27] drives a  $\sim 3\times$  reduction in the magnitude of the negative log-likelihood between epochs 1 and 50, after which it plateaus. Gradient norms (clipped at 5) fall by an order of magnitude over the same window. Early stopping was not used; we report the epoch-50 checkpoint. The adjacency mixture weights converge from initialisation (0.40, 0.35, 0.25) to (0.42, 0.34, 0.24), a small movement that is consistent with the prior alignment.

## E Reproducibility Notes

All numerical results in the paper are reproducible from the artefacts in the project repository at <https://github.com/kcbir/zcsc>. Inputs and seeds are fully deterministic; we list the relevant invariants for transparency.

*Software stack.* Python 3.11, PyTorch 2.2 (CPU build, `torch.use_deterministic_algorithms(True)`), NumPy 1.26, sentence-transformers 2.7, rust 1.77 (stable) for the ingestion edge, criterion 0.5 for benchmarks. All MPS / CUDA acceleration is disabled at runtime to guarantee bitwise reproducibility on Apple M2.

*Seeds.* A single seed of value 42 is used for numpy, torch and Python’s random. The random target baseline averages over 50 independent re-seedings (43, . . . , 92) so that its precision estimate inherits a low variance.

*Splits.* The temporal holdout is constructed by sorting all 638 events by timestamp and assigning the first 60% to warm-up (used to grow the c-LSTM state and to estimate the per-ticker percentile thresholds) and the last 40% to evaluation. No event from the holdout window participates in threshold estimation, eliminating same-day and forward-looking leakage.

*Hardware.* Apple M2 system-on-chip (8-core AArch64; 4 performance cores at 3.49 GHz and 4 efficiency cores at 2.42 GHz; 8 GB unified LPDDR5-6400 at 100 GB/s memory bandwidth; 512 GB NVMe SSD). All Rust benchmarks are compiled with `-C target-cpu=native -C opt-level=3` and run under criterion with default warm-up (3 s) and measurement windows (5 s).

*Note on camera-ready numbers.* Minor numerical differences from the submission draft reflect a post-review code cleanup; all camera-ready numbers are from the final deterministic checkpoint.

## F Per-Sector Detection Performance

Table 5 disaggregates contagion-detection precision at the 90th percentile by the GICS (Global Industry Classification Standard) sector of the source ticker. A single article can produce more than one source event when its text mentions several primary tickers (one fires per mention), which is why the per-sector counts  $n$  sum to more than the 638 articles in the corpus; the totals are reported per source-event, not per article. Sector-level sample sizes remain small in a one-month evaluation, so the table is reported as supporting evidence rather than a hypothesis test; we publish the breakdown to make the sector-conditional behaviour of the model fully visible.

**Table 5.** Detection precision at the 90th-pct threshold, conditioned on the source ticker’s GICS sector.  $n$  counts source events from that sector in the holdout window.

Source sector	$n$	Precision	Lift vs. Random
Information Technology	412	0.168	1.89×
Communication Services	86	0.156	1.75×
Consumer Discretionary	217	0.149	1.67×
Industrials	158	0.146	1.64×
Health Care	197	0.142	1.60×
Financials	263	0.139	1.56×
Energy	102	0.137	1.54×
Materials	74	0.130	1.46×
Consumer Staples	91	0.128	1.44×
Utilities	46	0.121	1.36×
Real Estate	39	0.115	1.29×
<b>All sectors</b>	<b>1685</b>	<b>0.151</b>	<b>1.70×</b>

The Information Technology sector shows the strongest lift, which is consistent with July 2022 being a month dominated by semiconductor-shortage and Fed-driven technology repricing narratives; sectors with thinner news flow and weaker pairwise co-mention links (Real Estate, Utilities) show comparatively smaller lifts. Even so, every sector clears the random baseline, and no sector’s precision falls below 0.115.